High-Resolution Near-Infrared Spectroscopy of H_3^+ Above the Barrier to Linearity

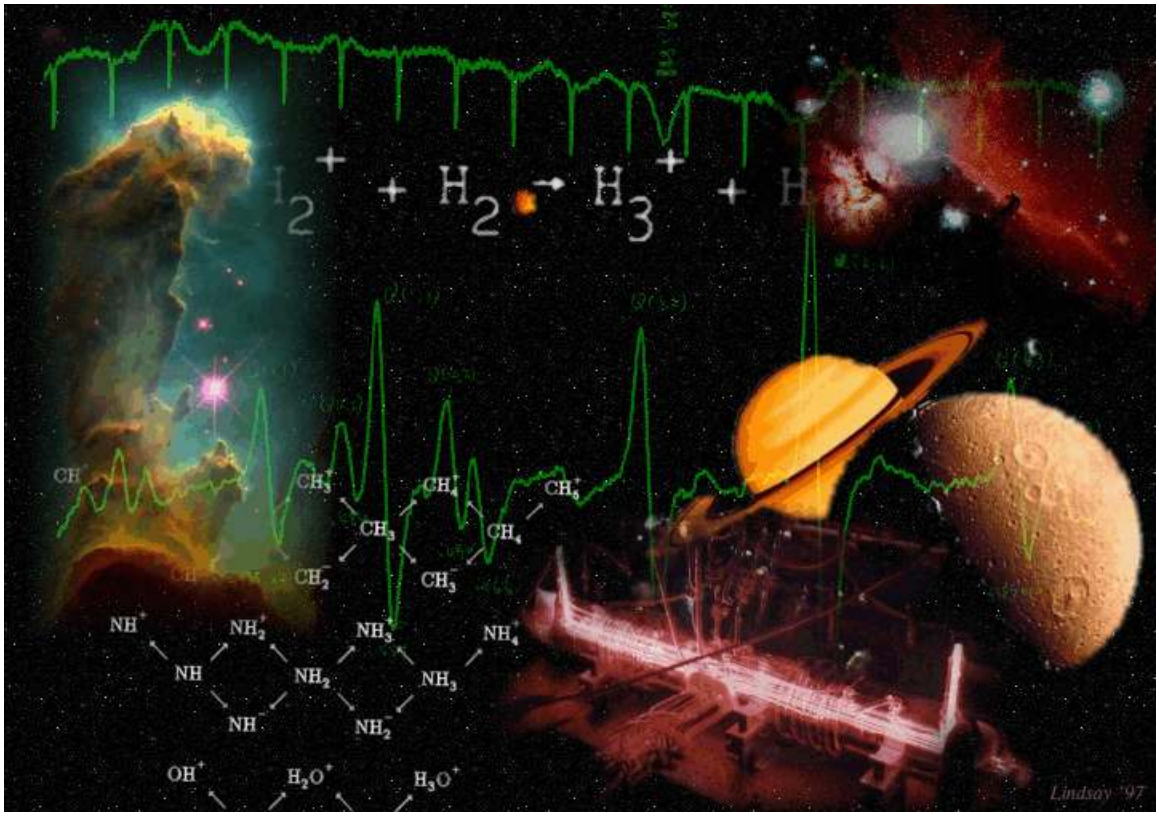

Jennifer Gottfried

Oka Ion Factory
October 29, 2001

Candidacy Committee: Butler, Guyot-Sionnest, Levy

Critical Review: “Photodynamics of ethylene: ab initio studies of conical intersections” M. Ben-Nun, T.J. Martinez Chem. Phys. 259, 237 (2000).

1 Introduction

H_3^+, consisting of three protons bound by two electrons, is the simplest polyatomic molecule. J. J. Thomson first established the existence of H_3^+ in 1911 using an early version of mass spectroscopy [1]. He identified an ion with a 3:1 mass-to-charge ratio, which he concluded was H_3^+, despite the prevailing conception that the hydrogen atom was always associated with exactly one electron. In 1916 Dempster demonstrated that H_3^+ was the dominant ion in hydrogen discharges [2]. As a result, H_3^+ is present in any environment where molecular hydrogen gas is ionized: electrical discharges, planetary ionospheres, and the interstellar medium. Since hydrogen makes up 92.1% of the known matter in the universe, H_3^+ plays a vital role in astrophysics.

One of the initial motivations for the laboratory spectroscopy of H_3^+ was to facilitate its astronomical study. As one of the major positive charge carriers in interstellar clouds, H_3^+ plays a fundamental role in the chemistry of the interstellar medium. In the ion-neutral reaction schemes introduced by Herbst and Klemperer [3] and Watson [4] in the early 1970s, H_3^+ played a dominant role as the "universal protonator" and the initiator of interstellar chemistry. The infrared absorption spectrum of H_3^+ was first observed in the laboratory by Oka in 1980 [5]. Trafton *et al.* made the first non-terrestrial observation of H_3^+ in the ionosphere of Jupiter in 1987, although it was not positively identified until 1989 [6]. Since then, many additional H_3^+ spectra have been recorded, both in the laboratory and in space – and H_3^+ has been the focus of numerous reviews [7-14].

In addition to its astronomical importance, H_3^+ serves as a benchmark for first principle quantum mechanics calculations of polyatomic molecules. An important interdependence between theory and experiment exists for H_3^+ – theoretical calculations help the experimentalists search for new transitions, and accurate experimental frequencies give theorists the ability to improve the various potential energy surfaces and variational calculations. In this prospectus, I propose complementary laboratory investigations of overtone and combination bands of H_3^+, beyond the barrier to linearity and higher in energy than any previously detected transitions. These transitions, which are ~4600 times weaker than the fundamental band, occur in the near-infrared region. The detection of these transitions requires the development of a high-resolution, high-sensitivity spectrometer. While the high energy levels (>10,000 cm^{-1}) at the focus of this work are unlikely to be observable in astronomical plasmas, the primary motivation for

continuing the study of vibrational states beyond those spectroscopically probed to date is to assist in the development of theoretical calculations of H_3^+. The energy levels to be studied are in a regime where the theory is expected to breakdown. Experimentally determined energy levels are therefore essential for evaluating the various techniques for fitting the potential energy surfaces, calculating the energy levels to spectroscopic accuracy, and treating the non-adiabatic and relativistic effects.

2 Background: Theoretical Calculations

In the last 25 years, H_3^+ has been the subject of numerous electronic structure calculations. Just as molecular hydrogen serves as a model for diatomic molecules, H_3^+ is used as a benchmark for theoretical calculations of polyatomic molecules using first principle quantum mechanics [15-17]. Using an *ab initio* potential energy surface, Carney and Porter [18] were the first to calculate the rovibrational energies of H_3^+ in 1976. In 1980 they calculated the rovibrational energy levels using a spectroscopically adjusted potential energy surface (several spectroscopic constants were fitted to new experimental data [5]), reducing their errors by an order of magnitude [19]. Meyer, Botschwina, and Burton [20] also calculated a semi-empirical *ab initio* potential, which has been used often in the calculation of H_3^+ energy levels. Röhse *et al.* [21] calculated the first purely *ab initio* potential energy surface of spectroscopic accuracy (i.e., errors less than 1 cm^{-1}) in 1994. The most accurate potential to date, however, is that of Cencek *et al.* [22], who calculated non-Born-Oppenheimer adiabatic and relativistic corrections. The development of better *ab initio* and semi-empirical potential surfaces has considerably improved the agreement between experiment and theory.

The application of the variational formalism by Sutcliffe and Tennyson [23] was also an important step in improving the accuracy of the calculated rovibrational energy levels. The power of the variational approach is that the rotational kinetic energy operator is known exactly, and can, in principle, be calculated for any value of J – unlike the effective Hamiltonian approach used in earlier calculations [19, 24], which provides reasonable energy levels for low J only (J<6). In this approach, the electronic Schrödinger equation is solved at a set of fixed nuclear configurations, and the resulting eigenvalues provide the potential energy surface (PES). Correction terms to this approximation are then introduced by perturbation theory. Because the electronic and nuclear coordinates are coupled through Coulombic interaction, the complete

separation of nuclear and electronic motion is never possible. Many different groups have developed various adiabatic, non-adiabatic, and relativistic corrections to the zeroth-order Hamiltonian. A recent paper by Lindsay and McCall [14] summarizes the different theoretical approaches and their validity below 9000 cm^{-1}.

The energy regime above the barrier to linearity is particularly difficult theoretically – until quite recently, few of the rovibrational variational calculations performed in this range included the correct boundary conditions for linear geometries. The equilibrium structure of H_3^+ is an equilateral triangle, but the angle θ (see figure 1) gradually increases with increasing energy until the molecule is able to sample linear configurations at the potential barrier (at $\theta = \pi$).

Figure 2 shows a one-dimensional slice of the Röhse *et al.* [21] potential energy surface calculated by forcing *r* and *R* to be equal, but allowing their magnitudes to change for each value of θ (in order to find the minimum energy). Above the barrier to linearity the molecule has enough vibrational energy to sample both halves of this potential slice, and the density of vibrational states increases dramatically.

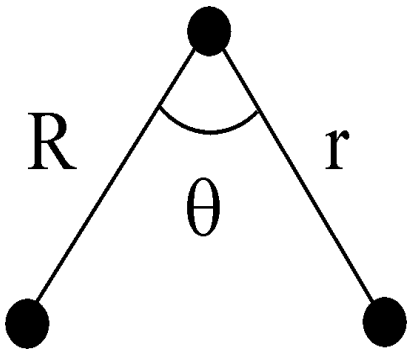

Figure 1. Scattering coordinates.

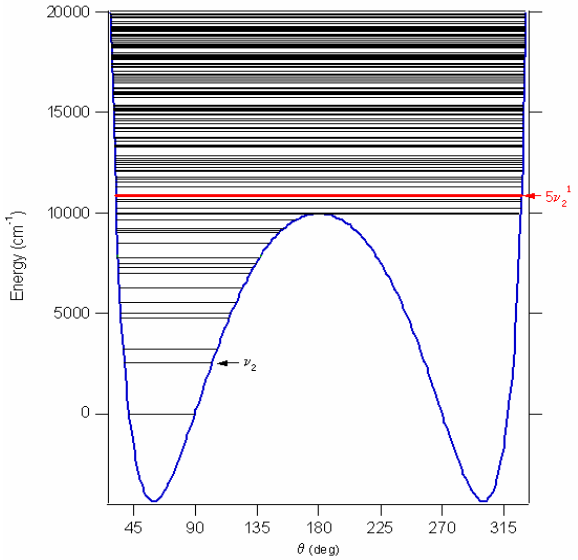

Figure 2. One-dimensional slice of the Röhse *et al.* [21] potential energy surface, including the *J*=0 vibrational energy levels.

When large-amplitude vibrational motion distorts the molecule into a linear configuration, it loses one of its moments of inertia. Because the rotational kinetic energy is inversely proportional to the moments of inertia of the molecule, a singularity occurs in the Hamiltonian. A careful choice of coordinate system and basis set ensures that this singularity does not cause any numerical problems, and enables the efficient computation of energy levels. Watson [17], Tennyson [25], and Alijah [28] have developed different approaches to

dealing with the ability of H_3^+ to sample linear configurations. These approaches are expected to produce energy levels of varying accuracy [21]. Comparison of the predicted energy levels to experimental energy levels will provide confirmation of the efficacy of the various coordinate systems and basis sets used to circumvent the singularity problem.

3 Production and Detection of H_3^+

All of the IR-active triply excited vibrational states (as well as those lower in energy) have been studied ($v_2, v_1, 2v_2^0, 2v_2^2, v_1+v_2, 3v_2^1, v_1+2v_2^2, 2v_1+v_2$). Due to the limitations of the laser, we decided to skip the third overtone ($4v_2^2 \leftarrow 0$) and search for the fourth overtone, $5v_2^1 \leftarrow 0$. Figure 3 shows the spectrum of the predicted transitions that I will search for. Although the fourth overtone is five times weaker than the third overtone band [26], the transitions associated with this band lie in a region where the laser has high power and good stability. Since the $5v_2$ vibrational energy level is fully above the linearity barrier (figure 2), the detection of the $5v_2^1 \leftarrow 0$ band is particularly important for assessing the accuracy of theoretical calculations above the barrier to linearity.

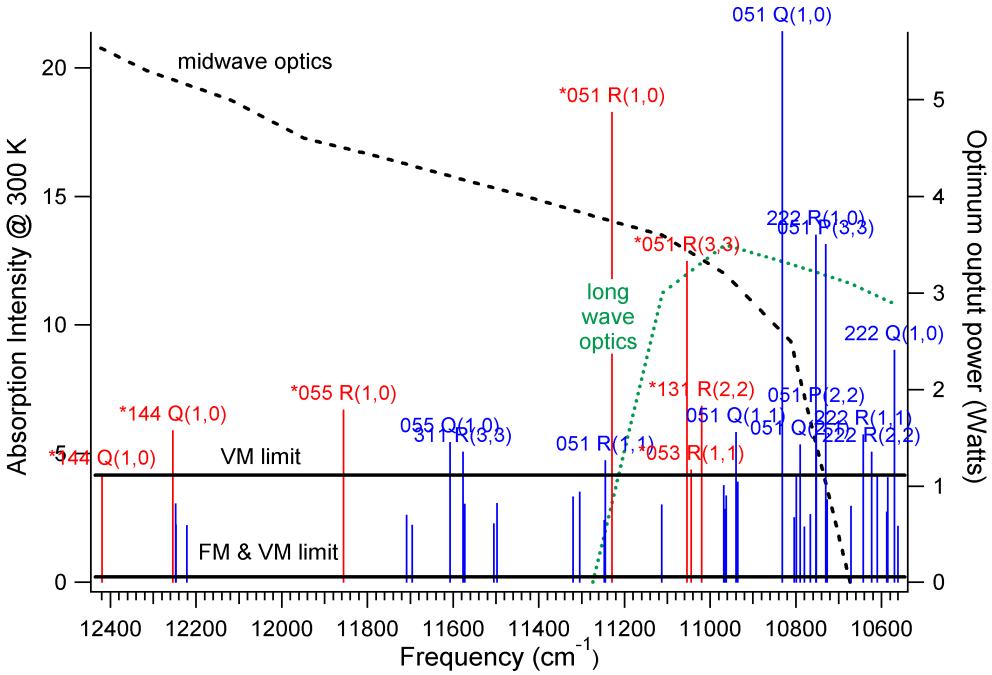

Figure 3. The tuning curves for two of the optics sets of the Ti:sapphire laser and the predicted spectrum of H_3^+ overtone and combination bands above the barrier to linearity. Also shown are the experimentally determined sensitivity limit for velocity-modulated detection and the theoretical sensitivity limit for frequency- and velocity-modulated detection (described below).

While overtone bands are usually much weaker than the fundamental because of smaller transition moments, the decrease in the transition moment of H_3^+ is less drastic than for heavier molecules, due to the extreme anharmonicity of the H_3^+ potential. Since the $5\nu_2$ band is approximately 4600 times weaker than the fundamental ν_2 band [26], which is about eight percent deep under similar experimental conditions [5], we anticipated that the strongest line of $5\nu_2^1 \leftarrow 0$ would have a fractional absorption of about 10^{-5}. Therefore, in order to detect a transition with a signal-to-noise (S/N) of 10 under these conditions, we would need a sensitivity (minimum detectable absorption $\Delta I/I$) on the order of 10^{-6}. Because the strongest line in the $\nu_1 + 2\nu_2^2 \leftarrow 0$ band (infrared region), which is about 17 times stronger than the $5\nu_2^1 \leftarrow 0$ band, was recently detected in our group under similar conditions [28] with a S/N of 100 and a sensitivity of $3*10^{-6}$, we could reasonably expect to see a fractional absorption of about 10^{-5} with good S/N by expanding the experimental techniques used in the infrared region to the near-infrared region.

The experimental apparatus described in this section has recently been assembled and used to take preliminary data. Although the Oka group is quite proficient at the production and detection of H_3^+, this particular laser system has not been used for gas phase spectroscopy in our group. Also, the high sensitivity recently achieved has never been obtained in this wavelength region by the Oka group.

3.1 Plasma cell

A liquid-nitrogen cooled discharge tube (as seen in figure 4) is used to produce the hydrogen discharge, the source of H_3^+. Approximately 500 mTorr of H_2 flows continuously into the central bore (1 m long, 18 mm diameter) through multiple gas inlets. A mechanical pump connected to the central bore keeps the gas inside the cell fresh by drawing the flow of reagent gas through the outlet tubes. The outermost jacket is evacuated to provide thermal insulation for the liquid nitrogen. Two CaF_2 windows mounted at the appropriate Brewster angle minimize reflection losses as the laser beam enters and exits the plasma cell.

An alternating current of about 310 mA at approximately 19 kHz is applied to the electrodes, located at each end of the cell. The applied potential is produced by a step-up transformer driven by a power amplifier. The resulting plasma is a non-equilibrium system with a rotational temperature of ~300K. These discharge conditions lead to H_3^+ column densities (concentration × absorption path length) on the order of 10^{14} cm^{-2}.

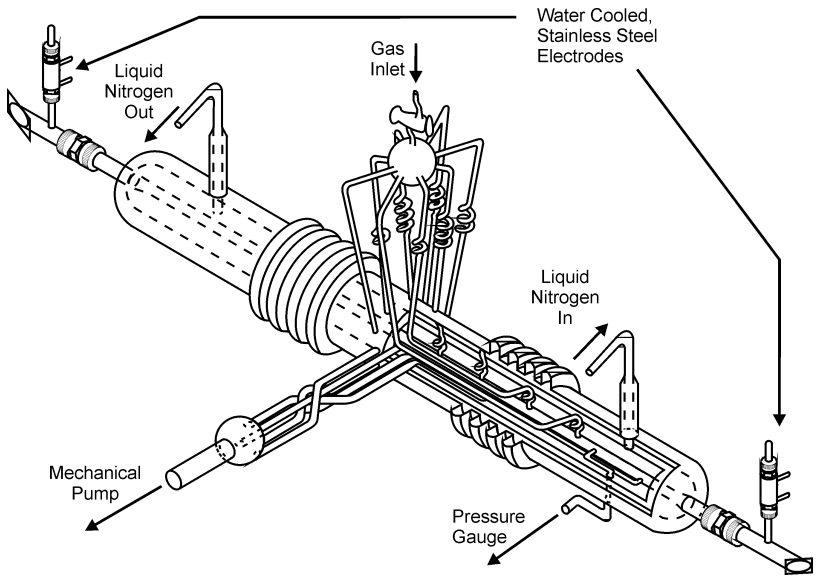

Figure 4. The liquid-nitrogen cooled discharge cell.

3.2 Laser System

A titanium:sapphire ring laser pumped by an argon ion laser provides approximately 1 W of continuous power, high spectral purity (500 kHz bandwidth), and a wide tuning range. Three interchangeable optics sets provide continuous coverage from 700-1050 nm. The laser is computer controlled and can scan over wide regions at lower sensitivity, or repetitively over smaller regions (~24 GHz) at higher sensitivity. Both integration and co-addition are used to improve the sensitivity.

3.3 Modulation Techniques

Modulation is a common technique used to minimize noise and baseline drift. In an experiment employing lasers, the primary source of noise is the intensity noise of the laser, which is much worse at low frequencies. By detecting the absorption signal at a frequency where $1/f$ noise is negligible, the sensitivity of the spectrometer can be greatly improved. This section describes the two modulation techniques used in our setup to maximize the sensitivity.

3.3.1 Velocity Modulation

A convenient way to modulate the signal is to produce the plasma discharge in an ac electric field. As the potential across the electrodes periodically reverses direction, the molecular ions are pulled back and forth along the axis of the plasma tube. The ions experience transition frequencies alternately Doppler-shifted either to the red or to the blue (from the laboratory frame

of reference). The absorption of laser radiation tuned to the resonant transition frequency is therefore amplitude modulated at the discharge frequency. This absorption signal can then be demodulated with a phase-sensitive detector (PSD) locked-in to the frequency of the discharge. This technique, known as velocity modulation [29], produces a first derivative lineshape.

The primary benefit of velocity modulation is the discrimination between ions and neutrals, since the more abundant neutrals will not be driven by the changing potential. Positive and negative ions are modulated and will appear with opposite phase, since they will be accelerated in opposite directions in a given potential. Given the low concentration of molecular ions in the plasma, this technique provides a tremendous advantage while studying weak transitions of ions in congested regions containing absorption signals of neutral molecules.

3.3.2 Frequency Modulation

A second, extremely powerful modulation technique used in our apparatus is frequency modulation (FM), also known as optical heterodyne spectroscopy [30]. In this technique, the single-mode laser is passed through a phase-modulating crystal called an electro-optic modulator (EOM), and an amplified radio frequency field is applied. The applied electric field induces a change in the refractive index of the crystal. As a result, the EOM produces optical sidebands that are separated from the optical carrier by the modulation frequency.

As the laser frequency is tuned, the spectral feature of interest is probed not only by the carrier frequency of the laser, but also by both FM sidebands. The absorption associated with the spectral feature can be measured by monitoring the phase and amplitude of the radio frequency heterodyne beat signal that occurs when the FM spectrum is distorted by the effects of the spectral feature on the probing sidebands. In the absence of an absorption signal, the beat frequencies of the sidebands exactly cancel each other. A spectral feature that is both velocity-modulated and frequency-modulated will appear (approximately) as a second derivative lineshape. Heterodyne detection has been a common technique in the microwave region for many years, and has become increasingly important in other wavelength regions. Figure 5 shows a schematic of our heterodyne detection electronics, including an EOM with a modulation frequency of 500 MHz.

Because single-mode lasers such as the Ti:sapphire have little noise at radio frequencies, the beat signals can be detected with a high degree of sensitivity. Ideally, the sensitivity should

be limited only by shot noise at the photodetector. Unfortunately, noise in the electronics of the detector limits the sensitivity in this spectrometer, so that the sensitivity-limit for this spectrometer under these experimental conditions is approximately $1.8*10^{-8}$.

3.4 Unidirectional Multipassing

In order to increase the depth of absorption, we want to make the absorption path length as long as possible. By passing the laser beam through the discharge cell multiple times, we can increase our path length by an order of magnitude or more. To avoid canceling out the velocity modulation signals, the beam must be passed through the cell in the same direction each time. We are limited by reflection losses to six passes through the cell in one direction. As long as the unidirectional nature of the multipassing is maintained, however, two separate beams can counter propagate through the cell, as described below.

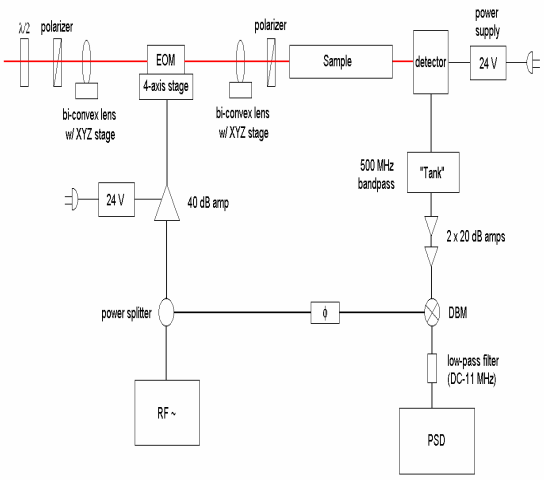

Figure 5. Schematic of the heterodyne detection electronics.

3.5 Noise Subtraction

The modified White cell configuration we use to multipass allows us to send a second beam through the discharge tube in the opposite direction of the first beam, while maintaining the unidirectional nature of the individual beams. Since the second beam travels in the opposite direction, it experiences molecular absorptions 180º out of phase with respect to the first beam. By balancing the optical power of the two beams and using a fast photoreceiver (650 MHz bandwidth) with two photodiodes, we can further reduce our noise by subtracting the two beams. The laser noise will cancel out, and the double-modulated signal will approximately double in intensity as the path length effectively doubles. Figure 6 shows a schematic of the entire apparatus described thus far.

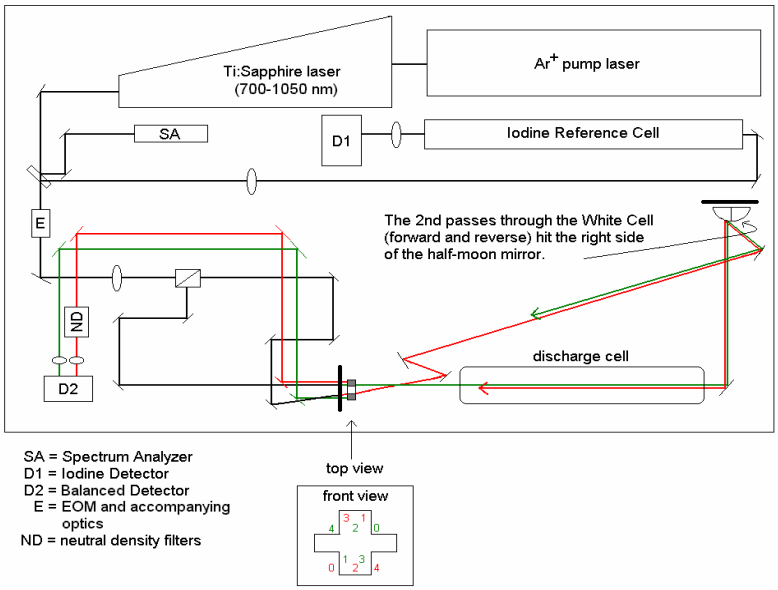

Figure 6. This high-resolution, high-sensitivity, near-infrared spectrometer is currently being assembled.

4 Summary of Recent Results

With the techniques described above (without frequency modulation), we have been able to identify seven new transitions above the barrier to linearity (marked in red in figure 3). After observing these transitions using velocity modulation at a sensitivity of $3*10^{-6}$, we realized we needed to improve our S/N in order to increase the number of detectable transitions. By adding frequency modulation to the spectrometer, the S/N (of an N_2^+ reference line) improved by a factor of 20 (see figure 7).

5 Conclusions

Although I have recently finished assembling the main components of the spectrometer, there are many subtleties to the detection scheme that have not yet been worked out, leaving room for improved sensitivity (the current sensitivity is approximately five times the theoretical sensitivity for this spectrometer) and a greater understanding of the system. The next step is to return to H_3^+ and record cleaner spectra of the previously seen transitions. Then, with the improved sensitivity I should be able to detect an additional 30 or more lines. By comparing the experimentally determined energy levels to the calculated energy levels of Alijah [27], Tennyson [25], and Watson [32] the efficiency of the various corrections to the Born-Oppenheimer

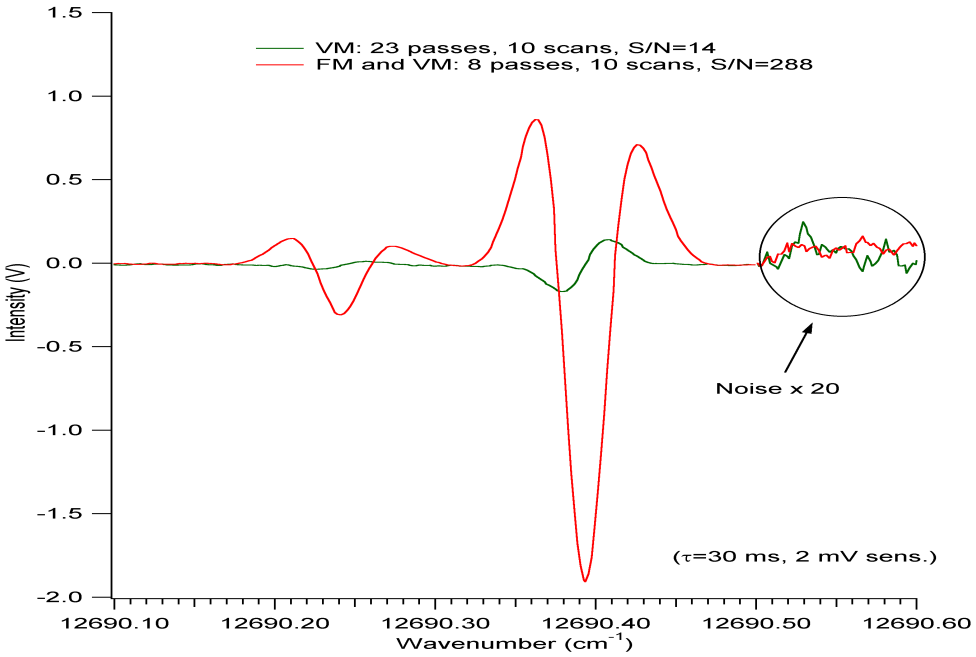

Figure 8. This figure compares the velocity-modulated signal of N_2^+ and the double-modulated signal. The smallest line is the $P_{21}(16)$ transition of the (2,0) vibrational band of the Meinel system $A^2\Pi_u$-$X^2\Sigma_g^+$, while the larger signal is the $Q_{22}(16)$ transition. The signal-to-noise ratios were calculated from the $P_{21}(16)$ transition – which is comparable in intensity to the $5\nu_2$ $R(1,0)$ line of H_3^+.

approximation and the validity of the different choices of coordinate systems and basis sets can be evaluated.

It should be emphasized that the H_3^+ transitions I propose to study are extremely weak. The high sensitivity achieved with our spectrometer can be used for detecting spectra of many other ions, including CH_2^+ and NH_2^+. Also, this work can be extended to higher overtone bands of H_3^+ ($6\nu_2^2 \leftarrow 0, 7\nu_2^1 \leftarrow 0$, etc.), continuing the climb up the energy ladder of H_3^+ and further testing the theoretical predictions and potentials. The lack of assigned spectroscopic data in the intermediate energy regime (from 10,000-35,000 cm^{-1}) means that the potential is not strongly constrained [33]. Consequently, none of the potential energy surfaces near the H_3^+ dissociation limit (~35,000 cm^{-1}) are considered reliable, and experimental data on higher energy levels is needed to improve them. An improved PES might finally enable the analysis of the near-dissociation spectra, which has remained completely unassigned since its initial discovery by Carrington *et al.* [34], almost 20 years ago.

6 References

1. J.J. Thomson, *Phil. Mag.* **24**, 209 (1912).
2. A.J. Dempster, *Phil. Mag.* **31**, 438 (1916).
3. E. Herbst and W. Klemperer, *Astrophys. J.* **185**, 505 (1973).
4. W.D. Watson, *Astrophys. J.* **183**, L17 (1973).
5. T. Oka, *Phys. Rev. Lett.* **45**, 531 (1980).
6. L. Trafton, D.F. Lester, and K.L. Thompson, *Astrophys. J.* **343**, L73 (1989).
7. T. Oka, *Rev. Mod. Phys.* **64**, 1141 (1992).
8. J. Tennyson and S. Miller, *Contemp. Phys.* **35**, 105 (1994).
9. J. Tennyson and S. Miller, *Chem. Soc. Rev.* **21**, 91 (1992).
10. A. Dalgarno, *Adv. At. Mol. Opt. Phys.* **32**, 57 (1994).
11. I.R. McNab, *Adv. Chem. Phys.* **89**, 1 (1995).
12. J. Tennyson, *Rep. Prog. Phys.* **57**, 421 (1995).
13. B.J. McCall, *Philos. T Roy. Soc. A* **358**, 2385 (2000).
14. C.M. Lindsay and B.J. McCall, *J. Mol. Spectrosc. in press* (2001).
15. R. Jacquet, *et al.*, *J. Chem. Phys.* **108**, 2837 (1998).
16. O.L. Polyansky and J. Tennyson, *J. Chem. Phys.* **110**, 5056 (1999).
17. J.K.G. Watson, *Chem. Phys.* **190**, 291 (1995).
18. G.D. Carney and R.N. Porter, *J. Chem. Phys.* **65**, 3547 (1976).
19. G.D. Carney and R.N. Porter, *Phys. Rev. Lett.* **45**, 537 (1980).
20. W. Meyer, P. Botschwina, and P. Burton, *J. Chem. Phys.* **84**, 891 (1986).
21. R. Röhse, *et al.*, *J. Chem. Phys.* **101**, 2231 (1994).
22. W. Cencek, *et al.*, *J. Chem. Phys.* **108**, 2831 (1998).
23. B.T. Sutcliffe and J. Tennyson, *J. Chem. Soc. Faraday Trans.* **83**, 1663 (1987).
24. J.K.G. Watson, *J. Mol. Spectrosc.* **103**, 350 (1984).
25. J.K.G. Watson, *Phil. Trans. R. Soc. Lond. A* **358**, 2371 (2000).
26. L. Neale, S. Miller, and J. Tennyson, *Astrophys. J.* **464**, 516 (1996).
27. P. Bartlett and B.J. Howard, *Mol. Phys.* **70**, 1001 (1990).
28. F.T. Smith, *J. Math. Phys.* **3**, 735 (1962).
29. R.C. Whitten and F.T. Smith, *J. Math. Phys.* **9**, 1103 (1968).
30. B.R. Johnson, *J. Chem. Phys.* **79**, 1916 (1983).
31. L. Wolniewicz and J. Hinze, *J. Chem. Phys.* **101**, 9817 (1994).
32. Benjamin J. McCall, *Spectroscopy of H_3^+ in Laboratory and Astrophysical Plasmas*, in *Chemistry and Astronomy & Astrophysics*. 2001, University of Chicago: Chicago, IL.
33. A. Alijah, P. Schiffels, and J. Hinze, *manuscript in preparation* (2001).
34. B.J. McCall and T. Oka, *J. Chem. Phys.* **113**, 3104 (2000).
35. C.S. Gudeman, *et al.*, *Phys. Rev. Lett.* **50**, 727 (1983).
36. G.C. Bjorklund, *Opt. Lett.* **5**, 15 (1980).
37. R. Wang, *et al.*, *Chem. Phys. Lett.* **307**, 339 (1999).
38. J.K.G. Watson, *personal communication* (1996).
39. J. Tennyson, *et al.*, *Phil. Trans. R. Soc. Lond. A* **358**, 2419 (2000).
40. A. Carrington, J. Buttenshaw, and R.A. Kennedy, *Mol. Phys.* **45**, 753 (1982).